Presented at the 29th European PV Solar Energy Conference and Exhibition, 22-26 September 2014, Amsterdam, The Netherlands

THE POTENTIAL OF MULTICRYSTALLINE N-TYPE SILICON FOR HIGH EFFICIENCY SOLAR CELLS

Florian Schindler [a,b], Bernhard Michl [a], Andreas Kleiber [a], Heiko Steinkemper [a], Jonas Schön [a], Wolfram Kwapil [a,b], Patricia Krenckel [a], Stephan Riepe [a], Wilhelm Warta [a], and Martin C. Schubert [a]
[a] Fraunhofer Institut für Solare Energiesysteme, Heidenhofstr. 2, D-79110 Freiburg, Germany
[b] Freiburger Materialforschungszentrum, Albert-Ludwigs-Universität Freiburg, Stefan-Meier-Str. 21, D-79104 Freiburg, Germany
Ph +49 761 4588 5321, Fax +49 761 4588 9250, Email: florian.schindler@ise.fraunhofer.de

ABSTRACT: This work aims for assessing the efficiency potential of multicrystalline n-type silicon as base material for the production of high efficiency solar cells. To achieve this goal, a multicrystalline (mc) n-type and a mc p-type silicon block were produced from the same silicon feedstock under identical crystallization conditions, only differing in their type of doping. This allows for an investigation of the change in material quality and efficiency potential by switching the type of doping from p- to n-type. The material quality is investigated along the whole block height by means of photoluminescence imaging (PLI) of the diffusion length after different typical solar cell processing steps. An "Efficiency limiting bulk recombination analysis" (ELBA) furthermore allows for a prediction of the spatially resolved efficiency potential by combining injection dependent minority carrier lifetime images with PC1D cell simulations. This investigation reveals a considerably higher efficiency potential after typical solar cell processes along the whole block height of the mc n-type silicon compared to the mc p-type silicon.
Keywords: multicrystalline silicon, n-type, doping, VGF, resistivity, efficiency

1 INTRODUCTION

For the fabrication of high efficiency solar cells, high quality bulk material with low recombination activity is inevitable. As n-type silicon features certain electrical advantages compared to p-type silicon, like smaller capture cross sections for minority carriers of many transition metals and the absence of the boron-oxygen-related degradation, state of the art high efficiency solar cell concepts are mainly based on n-type silicon [1]. This includes the current efficiency world record solar cell by Panasonic, which features a conversion efficiency of 25.6% on n-type Cz-substrate [2]. Despite the basic electrical advantages of n-type silicon, research on multicrystalline n-type silicon is scarce. The influence of impurities on the material quality has been investigated in recent publications [3-5]. Also, high lifetimes [6], large diffusion lengths and a high efficiency potential have been reported [7]. Still, no high efficiency mc n-type silicon solar cells have been fabricated so far. This might be due to the more complex processing and the higher costs of high efficiency solar cell concepts, which makes them economically cost-effective only for very high material quality.

In this work we quantify the efficiency gain resulting from switching the type of doping from p- to n-type for different solar cell processes in mc silicon considering samples along the whole block height. To this end, two multicrystalline silicon blocks were produced under identical crystallization conditions using the same high purity feedstock and the same crucibles. This enables us to attribute the observed differences in material quality mainly to the doping type. Additionally, the investigation along the whole block height accounts for the variation in resistivity.

In the first part of the paper, the investigated material is specified and the characterization techniques and simulations are summarized. In the second part, the material quality is investigated in terms of diffusion lengths, before the efficiency potential is assessed and loss mechanisms are quantified in the third part.

2 MATERIAL AND METHODS

2.1 Crystallization

In order to evaluate the influence of the doping type on the efficiency potential of mc silicon, two G2 size mc silicon blocks were crystallized using the same high purity feedstock, the same crucible (and coating), and comparable crystallization conditions. The blocks were crystallized at Fraunhofer ISE in the same laboratory crystallization furnace adapted for the crystallization of G1 and G2 size silicon blocks. One block was doped with boron (p-type) and the other with phosphorus (n-type). Thus, we obtain two mc silicon blocks with a comparable impurity distribution, differing only in their type of doping. The blocks were cut into three bricks, and 125x125mm² wafers were cut from the brick "A_{middle}" as depicted in Fig. 1. By this we obtain wafers with an edge region affected by solid-state in-diffusion of impurities from the crucible at one side.

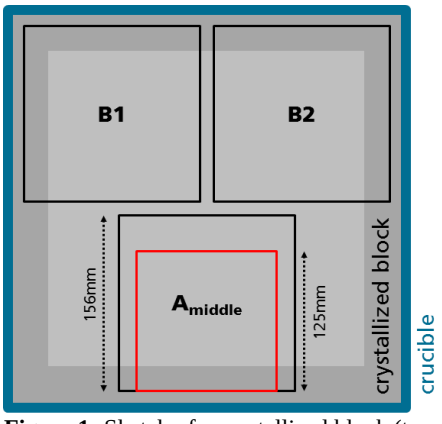

Figure 1: Sketch of a crystallized block (top view). 125x125mm² wafers were cut from the brick "A_{middle}" as depicted by the red frame. The edge region affected by solid-state in-diffusion of impurities from the crucible is indicated by the dark grey area

2.2 Sample processing

Wafers were selected from three positions along the block height, in the following denoted as "bottom", "middle", and "top". This allows for an investigation of the material quality along the whole block height of both blocks. The choice of identical block positions of the n- and p-type block ensures comparable impurity content within each group of wafers. For a prediction of the material efficiency potential, lifetime samples after typical high temperature steps of applicable solar cell concepts are required, as the material quality changes dependent on solar cell processing conditions. The wafers of both bricks were processed according to the scheme of Fig. 2. Each process includes wafers from all three block positions of both bricks.

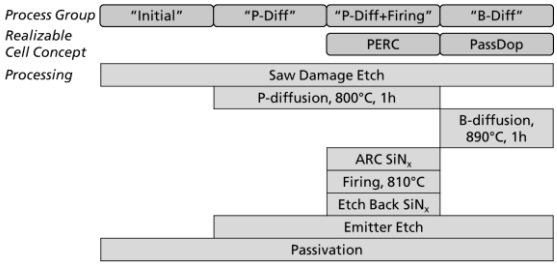

Figure 2: Sample processing

The steps of group "P-Diff+Firing" (phosphorus diffusion and firing) are representative for a PERC cell concept [8, 9] on a p-type base, those of the group "B-Diff" (boron diffusion) for a PassDop cell concept with low temperature metallization [10] on n-type. The group "P-Diff" serves as a reference group in order to investigate the impact of the firing step, the group "Initial" is included to assess the material quality before any high temperature processing.

2.3 Characterization techniques and simulations

The resistivity of both blocks was investigated by eddy current measurements at the block sides and by inductive measurements on wafer level. QSSPL-calibrated photoluminescence imaging (PLI) [11] was used for spatially resolved measurements of the diffusion length.

For a prediction of the material related efficiency potential, an "Efficiency limiting bulk recombination analysis" (ELBA) [12] with the modifications described in Ref. [13] was applied. Based on injection-dependent lifetime images and PC1D cell models, images of the material related solar cell efficiency potential can be calculated. The models for the cell simulations were chosen such that the efficiency limit without bulk recombination ("cell limit") is comparable for p- and n-type base material. This enables a direct comparison of both materials in terms of efficiency potential. For the simulations of the n-type material, the PassDop concept described in [10] in combination with a Honeycomb texture [14] is used, the simulations of the p-type material are based on a PERC concept [8, 9] with identical optics and dark saturation current densities for the front and the rear side as in the n-type model ($J_{0,rear}$ = 45 fA/cm², $J_{0,front}$ = 25 fA/cm²). As mentioned above, this choice of models leads to comparable cell limits for both materials, 21.7% for p-type and 21.8% for n-type.

The base resistivity variation for different block heights is accounted for in the PC1D cell models. Further details about the influence of the base resistivity will be part of a separate publication [15].

3 RESULTS

3.1 Resistivity

Besides the recombination properties of mc n- and p-type silicon, also the base resistivity is a crucial parameter influencing the solar cell efficiency potential. Fig. 3 shows the resistivity obtained from eddy current measurements at the block sides and inductive measurements at wafer level as a function of block height. The positions of the inductive measurements correspond to the three block positions (bottom, middle, top) investigated in this work.

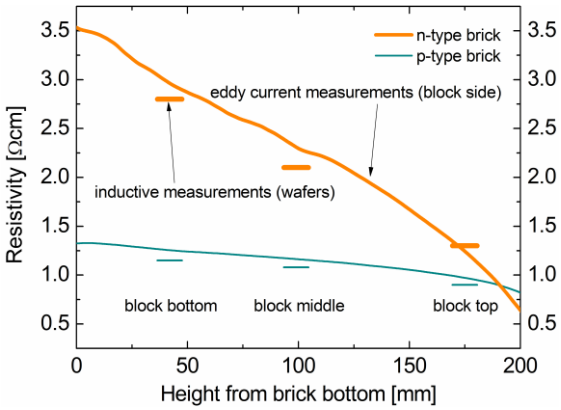

Figure 3: Resistivity

While the p-type brick shows a very low variation in resistivity, it strongly decreases with block height in the n-type brick. This is due to the lower segregation coefficient of phosphorus (0.35) compared to boron (0.8). The variation in the base resistivity is accounted for in the models used for the simulations of efficiency potential in section 3.3 as explained in detail in Ref. [15]. The differences between measurements on block and wafer level are attributed to lateral inhomogeneities due to a non-planar crystallization front and changing convection patterns in the silicon melt during crystallization on the one hand and to uncertainties in the measurement techniques on the other hand.

3.2 Diffusion length

For assessing the material quality after the different solar cell processing steps, we measured the spatially resolved minority carrier diffusion length by PLI. Comparing diffusion lengths instead of minority carrier lifetimes in mc n- and p-type silicon allows for a direct comparison of the material quality, as this already accounts for the lower minority carrier mobility in n-type. Fig. 4 shows the harmonically averaged diffusion length across the whole wafers for each block height and process step. The n-type brick features significantly larger diffusion lengths than the p-type brick after each solar cell process step along the whole block height. In the following, we will discuss the impact of the different processing steps on the material quality of p- and n-type silicon and its dependence on the block position.

In the p-type brick (shaded bars), the diffusion length increases after the phosphorus diffusion due to gettering of impurities, and is largest after the phosphorus diffusion with a subsequent firing step. This is attributed to a passivation of impurities by hydrogen from the silicon nitride stack during the firing [16].

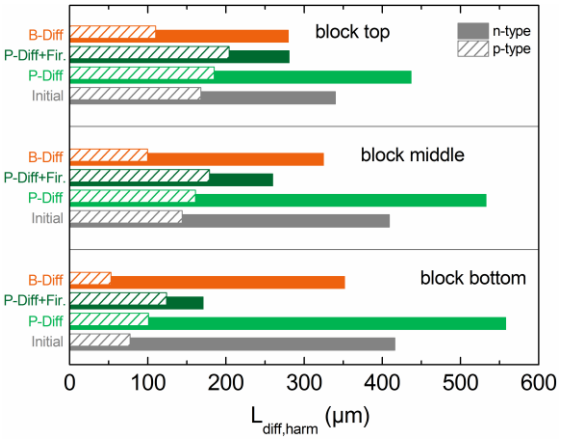

Figure 4: Diffusion length (harmonic mean across the whole wafers) of mc p- and n-type silicon after different solar cell processing steps at different block heights

Also the n-type material quality increases after the P-diffusion, while the subsequent firing step leads to a large reduction of diffusion lengths. This could be explained by the dissolution of initially large precipitates and redistribution to a higher density of smaller precipitates during the fast cooling to room temperature after the firing step. Another possibility could be a diffusion of formerly gettered impurities from the emitter into the bulk [17, 18]. Still, the diffusion length is larger than in the p-type material after any process step.

A boron diffusion harms the material quality of both mc p- and n-type silicon compared to the initial state, which can be due to the dissolution of precipitates at the high temperature of the B-diffusion (890°C) and the lower gettering efficiency compared to the P-diffusion (800°C). Still, the diffusion length in mc n-type silicon is on a high level after the B-diffusion (≥ 300 µm) and larger than in mc p-type silicon after any process step.

The material quality of the p-type brick shows a clear dependence on the block position. For all process groups, the diffusion length increases with block height. This can be attributed to the limitation of mc p-type silicon by homogeneously distributed recombination centers such as dissolved impurities. The concentration of dissolved impurities is largest in the areas affected by solid-state in-diffusion of impurities from the crucible. Wafers from the lowest block position are affected by solid-state in-diffusion from the crucible bottom and the crucible walls (edge region). As the solid-state in-diffusion from the crucible bottom only affects wafers from the lowest block position and the edge region narrows towards the block top, the material quality of the mc p-type block increases with block height.

In the mc n-type block, the opposite trend is observed, a decrease in diffusion length towards the block top. This is attributed to the limitation of mc n-type wafers by decorated crystal defects such as grain boundaries and dislocations. As the dislocation density increases towards the block top, the material quality decreases. An exception is the processing group "P-Diff+Firing". As mentioned before, the firing step strongly harms the material quality in the n-type wafers, probably due to a dissolution and redistribution of initially large precipitates or an in-diffusion of previously gettered impurities from the emitter. Thus, small precipitates or dissolved impurities with a comparable or even higher capture cross section for minority carriers in n-type silicon could limit the diffusion length after firing, which leads to the same dependence of block height as in the p-type brick.

Diffusion length images, which support the interpretation of the results of this section, can be found in Ref. [15].

3.3 Efficiency potential

In this section, the material quality is discussed in terms of solar cell efficiency potential. Therefore, injection dependent lifetime images were combined with PC1D simulations as explained in section 2.3. We compare the efficiency potential of p-type wafers from the group "P-Diff+Firing", which feature the best material quality of the p-type brick, with the efficiency potential of n-type wafers from the group "B-Diff". This allows for a fair-minded comparison of p- and n-type efficiency potentials, as the processing steps of both groups are representative for typical solar cell concepts on p- and n-type substrates as introduced in section 2.2. Additionally, we include the n-type wafers from the group "P-Diff", as these wafers feature the largest diffusion lengths. This enables us to assess the upper limit of the efficiency potential in the n-type brick. An advanced cell concept would have to be chosen to realize solar cells from n-type wafers after a P-diffusion without applying any further high temperature step. For example, this could be a cell structure with a low temperature emitter (e.g. a hetero structure).

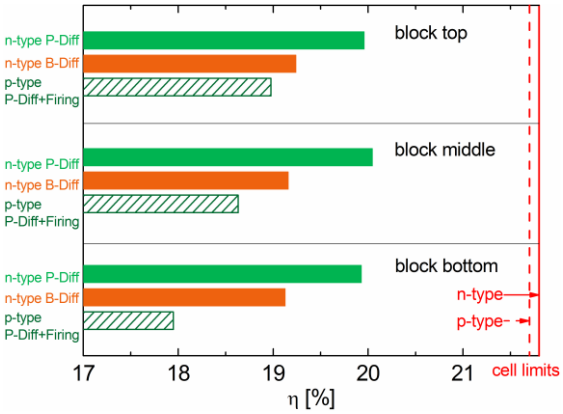

Figure 5: Global efficiency potential of the whole wafers (125x125 mm²)

Fig. 5 shows the efficiency potential of the three groups as a function of block height. While the efficiency potential of the p-type brick after P-Diff+Firing depends on the block height and increases from ~18% at the block bottom to ~19% at the block top, the n-type bricks features a larger and stable efficiency potential of ~19.2% along the whole block height after B-Diff. The largest efficiency potential of ~20% is achieved on n-type wafers after P-Diff along the whole block height. The dependence on the block position in the p-type bricks correlates with the material quality, which increases towards the block top as shown in the previous section. In the n-type brick, despite the decreasing material quality towards the block top, the efficiency potential is stable. This is due to the decreasing base resistivity, which leads to a higher efficiency potential as shown in Ref. [15], thus compensating the lower material quality. In a separate publication we show that the efficiency potential in the n-type brick could even be increased by an optimization of the resistivity [15].

In Fig. 6, which shows the spatially resolved ef-

ficiency potential for samples from medium block height, the different limitations in p- and n-type wafers become obvious. While the p-type sample is limited by homogeneously distributed recombination centers leading to an efficiency potential below 20% even in the best grains, the best 1x1 cm² in the n-type samples feature an efficiency potential of 21% after B-diffusion and 21.5% after P-Diffusion, which is close to the cell limit of 21.8%.

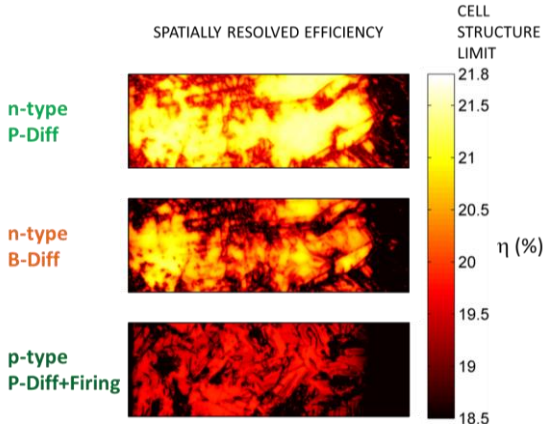

Figure 6: Spatially resolved efficiency potential for samples from medium block height. The images show the central stripe (125x31.25 mm²) of the wafers. The impact of the edge region close to the crucible is visible on the right side of the wafers

Fig. 7 highlights the efficiency gains obtained from mc n-type silicon after a B- or a P-diffusion compared to mc p-type silicon after P-Diff+Firing as a function of block height. The efficiency gain averaged for the three block positions is ~0.7%$_{abs}$ for n-type after B-Diff and ~1.5%$_{abs}$ for n-type after P-Diff for the material under test.

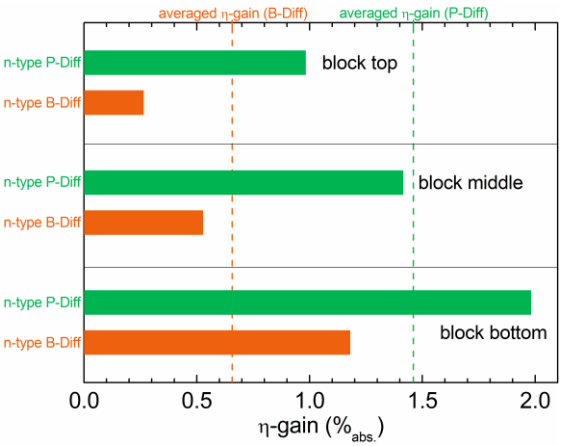

Figure 7: Efficiency gain of mc n-type silicon after B-diffusion or P-diffusion along the block height compared to mc p-type silicon after P-diffusion and firing

3.4 Efficiency loss analysis

While the previous part highlights the significant efficiency gain obtained from n-type doping, in this section the origins of efficiency losses are quantified. For this purpose, an ELBA analysis is performed in the best 1x1 cm² area of the wafers. Comparing the efficiency potential in these areas with the cell limit gives access to the limitations by homogeneously distributed recombination centers remaining in the bulk after processing. These homogeneously distributed recombination centers comprise impurities stemming from the feedstock and the in-diffusion from the crucible system into the silicon melt as well as impurities incorporated during processing. As discussed before, for the p-type wafer from the block bottom this also comprises impurities stemming from solid-state in-diffusion from the crucible bottom. These losses are depicted by the gray parts of the bars in Fig. 8. An ELBA analysis of the wafer excluding the edge region additionally takes into account losses due to structural crystal defects like dislocation clusters and grain boundaries (light gray dashed part of the bars in Fig. 8). Finally, comparing the efficiency potential of the whole wafer with the cell limit includes losses stemming from the edge region, which are highlighted by the black parts of the bars in Fig. 8.

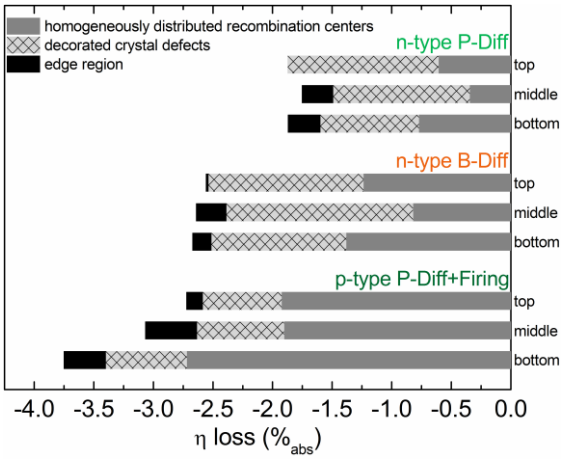

Figure 8: Efficiency losses

This analysis gives access to the different origins of efficiency losses in mc silicon. While in mc p-type silicon, the major part of the losses can be attributed to homogeneously distributed recombination centers in the good grains (> 60%), in mc n-type silicon structural crystal defects probably decorated with impurities are responsible for the main losses (~50% after B-Diff and ~60% after P-Diff, averaged along the block height). As mentioned before, especially after the P-diffusion efficiency losses in the best grains of the n-type wafers are very low and lead to an efficiency potential close to the cell limit in these areas (cf. Fig. 6).

4 CONCLUSION

In this work we assessed the efficiency potential of multicrystalline n-type silicon after typical solar cell processing steps in comparison to mc p-type silicon of comparable impurity level. An investigation along the whole block height revealed a significant average efficiency gain of 0.7%$_{abs}$ for mc n-type silicon after a boron diffusion and 1.5%$_{abs}$ for mc n-type silicon after a phosphorus diffusion compared to mc p-type silicon after a phosphorus diffusion and firing. We showed that the large efficiency gain can be attributed to the significantly lower impact of homogeneously distributed recombination centers on the material quality. The main source of ef-

ficiency losses in mc n-type silicon was found to be structural crystal defects probably decorated with impurities.

The efficiency potential of the p-type material shows a significant dependence on the block position correlated to the material quality. In contrast, despite the decreasing material quality towards the block top, the efficiency potential of the mc n-type silicon brick is stable along the whole block height. As shown in a separate publication [15], this is attributed to the decreasing base resistivity which leads to a higher efficiency potential and thus compensates the lower material quality.

ACKNOWLEDGEMENTS

This work was funded by the German Federal Ministry for Economic Affairs and Energy within the research project "THESSO" under contract number 0325491. The content is the responsibility of the authors.

REFERENCES

[1] M. A. Green, K. Emery, Y. Hishikawa, W. Warta, and E. D. Dunlop, Progress in Photovoltaics: Research and Applications **22** (7), 701 (2014).

[2] K. Masuko, M. Shigematsu, T. Hashiguchi, D. Fujishima, M. Kai, N. Yoshimura, T. Yamaguchi, Y. Ichihashi, T. Yamanishi, T. Takahama, M. Taguchi, E. Maruyama, and S. Okamoto, Proceedings of the 40th IEEE Photovoltaic Specialists Conference, Denver, Colorado, USA, 2014.

[3] J. Libal, Dissertation, Universität Konstanz, 2006.

[4] L. J. Geerligs, Y. Komatsu, I. Röver, K. Wambach, I. Yamaga, and T. Saitoh, Journal of Applied Physics **102** (9), 093702 (2007).

[5] G. Coletti, R. Kvande, V. D. Mihailetchi, L. J. Geerligs, L. Arnberg, and E. J. Øvrelid, Journal of Applied Physics **104**, 104913 (2008).

[6] A. Cuevas, M. J. Kerr, C. Samundsett, F. Ferrazza, and G. Coletti, Applied Physics Letters **81** (26), 4952 (2002).

[7] B. Michl, J. Benick, A. Richter, M. Bivour, J. Yong, R. Steeman, M. C. Schubert, and S. W. Glunz, Energy Procedia **33**, 41 (2013).

[8] A. W. Blakers, A. Wang, A. M. Milne, J. Zhao, and M. A. Green, Applied Physics Letters **55** (13), 1363 (1989).

[9] P. Engelhart, G. Zimmermann, C. Klenke, J. Wendt, T. Kaden, M. Junghänel, K. Suva, B. Barkenfelt, K. Petter, S. Hermann, S. Schmidt, D. Rychtarik, M. Fischer, J. W. Müller, and P. Wawer, Proceedings of the 37th IEEE Photovoltaic Specialists Conference, Seattle, Washington, USA, 2011.

[10] D. Suwito, U. Jäger, J. Benick, S. Janz, M. Hermle, and S. W. Glunz IEEE Transactions on Electron Devices **57** (8), 2032 (2010).

[11] J. A. Giesecke, M. C. Schubert, B. Michl, F. Schindler, and W. Warta, Solar Energy Materials and Solar Cells **95** (3), 1011 (2011).

[12] B. Michl, M. Rüdiger, J. Giesecke, M. Hermle, W. Warta, and M. C. Schubert, Solar Energy Materials & Solar Cells **98**, 441 (2012).

[13] B. Michl, M. Kasemann, W. Warta, and M. C. Schubert, Physica Status Solidi RRL – Rapid Research Letters **7** (11), 955 (2013).

[14] H. Hauser, B. Michl, S. Schwarzkopf, V. Kübler, C. Müller, M. Hermle, and B. Bläsi, IEEE Journal of Photovoltaics **2** (2), 114 (2012).

[15] F. Schindler, B. Michl, A. Kleiber, H. Steinkemper, J. Schön, W. Kwapil, P. Krenckel, S. Riepe, W. Warta, and M. C. Schubert, IEEE Journal of Photovoltaics, submitted (2014).

[16] R. Einhaus, F. Duerinckx, E. Van Kerschaver, J. Szlufcik, F. Durand, P. J. Ribeyron, J. C. Duby, D. Sarti, G. Goaer, G. N. Le, I. Périchaud, L. Clerc, and S. Martinuzzi, Materials Science and Engineering: B **58** (1–2), 81 (1999).

[17] J. Schön, M. C. Schubert, H. Habenicht, and W. Warta, Proceedings of the 25th European Photovoltaic Solar Energy Conference and Exhibition, Valencia, Spain, 2010.

[18] B. Michl, J. Schön, W. Warta, and M. C. Schubert, IEEE Journal of Photovoltaics **3** (2), 635 (2013).